

*Full Length Research Paper*

# Numerical and experimental evaluation of bearing capacity factor $N_y$ of strip footing on sand slopes

Mohd Raihan Taha\* and Enas B. Altalhe

Department of Civil and Structural Engineering, Universiti Kebangsaan Malaysia, 43600 UKM Bangi Selangor, Malaysia.

Accepted 09 September, 2013

Results of laboratory model tests and numerical studies on the behavior of a strip footing adjacent to a sand slope are investigated and presented in this paper. The investigated parameters include the effects of depth of the first reinforcement layer, vertical spacing, number of reinforcement layers, and distance between the edges of footings on bearing capacity. Results were analyzed to determine the effects of each parameter. Using a strip footing located near a sand slope crest had a significant effect on improving bearing capacity. The improvement increased when relative density decreased. The depth of the first layer decreased with further improvement when the distance of the footing edge from the slope crest increased. Using a strip footing can be considered effective in controlling the horizontal movement of the subgrade and in decreasing slope deformation. Finite element analysis explained and identified the failure pattern of strip footings adjacent to a slope crest. The findings also confirmed the load transfer mechanism and showed how a slope can be protected when geotextile is used.

**Key words:** Strip footing, slope stability, plaxis, bearing capacity, scale effects.

## INTRODUCTION

Rapid population growth and urbanization have resulted in increased construction areas and the decrease of suitable settlement areas. As a result, the bearing capacity and settlement criteria for building construction are changing. The use of unwanted soil has also become obligatory. Engineering structures, foundation systems, ground transportation, and living conditions are usually designed by using shallow foundations, which becomes problematic with regard to certain types of soil. The most commonly used solution is deep/pile foundation, which is applied by selecting the foundations of a building. Deep/pile solution is expensive. However, rapid advancements in construction technology that provide new solutions to problematic surfaces have made deep/pile solution necessary. Several methods in soil solution have been developed since the 1970s

and improved problematic soil strength properties. Economical methods based on deep foundation system solutions can be applied in certain cases. Geotechnics, which is a type of reinforced soil application, is one of the commonly used solutions. Reinforced soil application takes various resistant elements in the soil reinforcement placement depending on the obtained composite reinforcement material.

The concept of soil reinforcement was introduced in 1968 by French engineer Henri Vidal. Several theoretical and experimental geotechnical engineering studies have followed Vidal's proposal. Vidal (1968) implemented soil reinforcement by using a metal strip and reinforcing material. After the 1980s, along with technological advancement, the location of the metal strip used in synthetic geotextile and geogrid materials such as

\*Corresponding author. E-mail: [profraihan@gmail.com](mailto:profraihan@gmail.com) or [enasraft@yahoo.com](mailto:enasraft@yahoo.com). Tel: +603-89216218, Fax: +603-89216147.

polymer raw materials, was developed. Geotechnical engineering is practical and promotes the use of economical geosynthetic structures and materials. Thus, geotechnical engineering is increasingly applied to constructing dams, roads, landfills, and retaining structures.

Geotextiles and geogrids are the most commonly used geosynthetic materials in geotechnical application. Geotextiles enable more separation and filtration, and are used for drainage. Geogrids, which have lower metal rigidity, reduce ground transportation through strength and expected settlement. Although geogrids have a coupling effect with the ground through grid-shaped openings, these mechanisms tend to perform effectively.

Studies were conducted on flat-surfaced floors, foundation bearing capacity, and settlement behaviors based on improvement from using geogrid reinforcement (Binguet and Lee, 1975a; Akinmusuru and Akinbolade, 1981; Fragaszy and Lawton, 1984; Guido et al., 1985; Huang and Tatsuoka, 1990; Mandal and Sah, 1992; Dixit and Mandal, 1993; Khing et al., 1993; Yetimoğlu et al., 1994; Adams and Collin, 1997; Laman and Yildiz, 2003; Kumar and Saran, 2003; Michalowski, 2004; Kumar and Walia, 2006). However, in certain cases, foundations are constructed on or near slopes (bridge piers, utility poles, and buildings). In such cases, non-transportation capacity of the inclined surface decreases significantly.

In cases where the foundation is built on a slope, one of the solutions to increase bearing capacity is to place the foundation at a sufficient distance away from the top of the slope, which reduces the impact of transportation capacity. An alternative method is using transportation to increase geogrid reinforcement capacity. However, using transportation is not economical. A limited number of studies on strip foundation have been conducted. Selvedurai and Gnanendran (1989) and Lee and Manjunath (2000) used a single reinforcement layer and examined the effects of a strip foundation on the bearing capacity. Huang et al. (1994) started a research using geotextile reinforcement and it explained about failure mechanism on sand slope. Yoo (2001) and Laman et al. (2007) used a multi-layer case in their experimental studies. Bathurst et al. (2003) conducted a large-scale experiment to examine the failure mechanism. El Sawwaf (2007) investigated clay on the parameters of tapered equipment for sand filling. Previous analyses and experiments that mostly focused on single angle of slope, stability, and uniform basic width used geogrid reinforcement.

Moghaddas and Khalaj (2008) conducted an experimental study on the benefits of geogrids to the deformation of small-diameter pipes and settlement of the soil surface when subjected to repeated loads that simulate vehicle loading. According to the report, using geogrid reinforcement can significantly reduce the vertical diameter change of pipes and the soil surface settlement. El Sawwaf and Nazir (2010) conducted a laboratory study

on the effects of geosynthetic reinforcement on the cumulative settlement of repeatedly loaded rectangular model footings placed on reinforced sand. Repeated load tests were performed with different initial monotonic load levels to simulate structures. Live loads, such as petroleum tanks and ship-repair tracks, changed slowly and repeatedly.

Moghaddas and Dawson (2010) and El Sawwaf and Nazir (2012) studied repeated loads and cyclic loads, respectively, on model strip footings. A series of experiments were conducted to investigate the behavior of strip footings supported on three-dimensional and planar geotextile-reinforced sand beds subjected to repeated loads. The aforementioned researchers determined the effects of partial replacement of compacted sand layer and the inclusion of geosynthetic reinforcement. They found that the efficiency of sand-geogrid systems was dependent on cyclic load properties and on the location of the footing relative to the slope crest.

Scale effects between laboratory and field testing of footings were explored by a number of researchers (Berry, 1935; De Beer, 1963; Bolton and Lau, 1989; Das and Omar, 1994; Tatsuoka et al., 1994; Kusakabe, 1995; Kerry et al., 1999; Banimahd and Woodward, 2006; Cerato and Lutenegeger, 2007; Kumar et al., 2008; Chang et al., 2010). Scale effects were presented by Berry (1935), who showed that the bearing capacity of model circular footings increases disproportionately with increasing footing size (50.8, 71.8, 101.6, and 143.7 mm) on dense sand held at the same relative density. The bearing capacity factor  $N_{\gamma}$  decreases with increasing footing size  $N_{\gamma}$ . The bearing capacity can be calculated as follows:

$$q_{ult} = \frac{1}{2} \gamma' B N_{\gamma} \quad (1)$$

Generally, the bearing capacity factor ( $N_{\gamma q}$ ) from model footings depends on footing width  $B$ . The magnitude of  $N_{\gamma q}$  increases as the footing size decreases (De Beer, 1965; Das and Omar, 1994; Clark, 1998; Zhu et al., 2001; Lancelot et al., 2006; Cerato and Lutenegeger, 2007). The increase of  $N_{\gamma q}$  with the decrease of footing size becomes particularly extensive when the footing size becomes smaller than 1 m (Banimahd and Woodward, 2006). Kumar et al. (2008) conducted small-scale model tests with 7 cm strip footing and found that the value of  $N_{\gamma q}$  was extremely high. In the present paper, the footing size is only 5 cm. Thus, the value of  $N_{\gamma q}$  may be extremely high. Tatsuoka et al. (1991, 1994) reported that the scale effects were due to two factors: mean stress level beneath the footing and particle size. Bolton and Lau (1989) and Kusakabe (1995) stated that the particle size effect ( $B/d_{50\%}$ ) was insignificant to the results when ( $B/d_{50\%}$ ) was greater than 50 or 100. The value of ( $B/d_{50\%}$ ) is approximately 100 in the present study. Consequently,

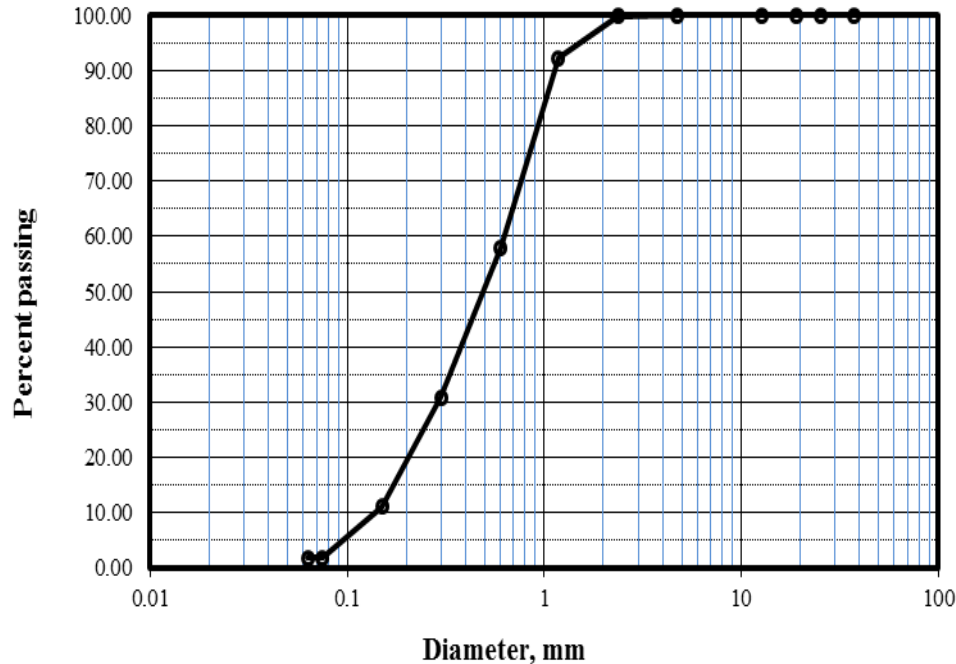


Figure 1. Grain size distribution of sand.

the particle size effect can be avoided. Unless the bearing capacity factor is modified, the effect of the first factor is difficult to account (Shiraishi, 1990). Kusakabe et al. (1991) showed that shape factor decreases by 33% as a footing size increases up to 3m.

In the present study, unreinforced, geotextile-reinforced, and increasing footing width  $B$  (unreinforced and reinforced) strip foundation bearing capacity, and settlement behavior of place on sandy slopes were investigated through laboratory model tests. In the unreinforced case, we studied the distance from the top of the foundation slope and the degree of stabilizing behavior of bearing capacity based on the effects of the parameters. In the reinforced case, the number of reinforcement layers and behavior of the parameters were investigated along with effects on bearing capacity factor. Based on the ratio of the distance from the slope crest to the footing width, basic size, and bearing capacity factor, we obtained the optimum reinforcement parameters. The effects of increasing footing width  $B$  in shear strength parameters were also experimentally determined in the unreinforced and non-woven geotextile-reinforced models for the availability of the fillings which was investigated. The availability of the fillings was determined by the value of the largest bearing capacity. In our study, unreinforced and reinforced foundations on the sand slopes were simulated by using computer software PLAXIS with two-dimensional and plane strain conditions. The numerical solution of the finite element method (FEM) was obtained. The results were compared with the experimental results.

## MATERIALS AND METHODS

### Tests on model footings

#### Test equipment

The apparatus used for the model tests consisted of a cuboid soil bin that measures 2,000 mm  $\times$  600 mm  $\times$  620 mm, a loading frame, a hydraulic jack, a pumping unit, and measuring devices for load settlement monitoring. The test tank was made rigid to prevent volume change during test bed preparation and during the load test. To accommodate the bearing ball, a 50 mm  $\times$  15 mm thick rigid steel footing with a notch hole at the top center was used as the model footing. The length of the steel footing was kept equal to the length of the tank (600 mm) to ensure the strip footing behavior and the plane strain condition. A controlled pouring and tamping technique was adopted to obtain the required unit weight of sand in the tank. The load was transferred to the footing by using a bearing ball, which produced a hinge. The hinge enabled the footing to rotate freely as it approached failure and eliminated any potential moment transfer from the loading fixture. Settlement of the footing was measured by using two mechanical dial gauges with least count of 0.01 mm. Medium coarse sand with grain size that ranges from 0.06 to 2.00 mm was used. Grain size distribution of the sand is shown in Figure 1. Optimum moisture content was determined by using a standard Proctor test and was found to be approximately 10%. Different relative densities of the sand were used by forming the designed weight of the sand into a certain volume of the soil bin by compaction.

#### Numerical modeling

Experimental results were verified through numerical modeling by using FEM. Plane strain elastoplastic finite element analysis (FEA) was conducted by using the commercial program PLAXIS 2D

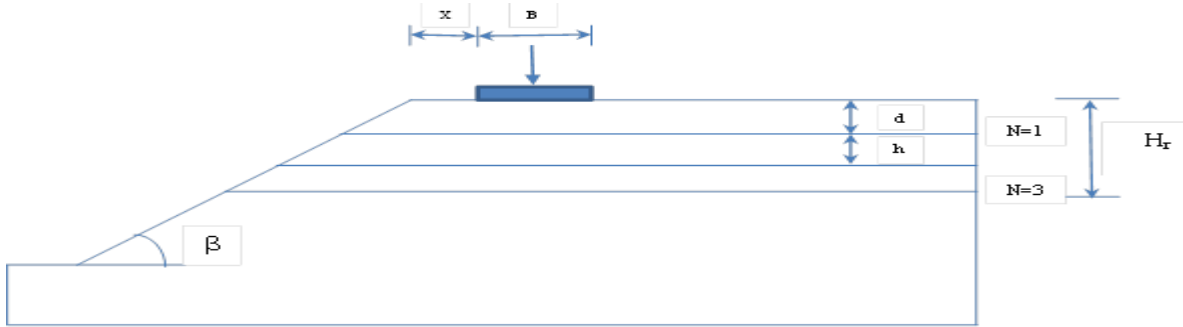


Figure 2. Slope geometry and parameters.

(Bringgreve and Vermeer, 1998; Plaxis, 2002). PLAXIS can address a wide range of geotechnical problems, such as deep excavations, tunnels, and earth structures (for example, retaining walls and slopes). Prototype slopes were supposed to rest on a yielding foundation and extend laterally to a distance of 1.5 times the slope height (H) from the toe of the slope. The initial conditions generally comprise the initial groundwater conditions, the initial geometry configuration, and the initial effective stress state. The sand layer was dry, which made implementing ground water condition unnecessary. However, the analysis required the generation of initial effective stresses via K0 procedure. The geometry of the prototype footing slope system was supposed to be similar to that of the laboratory model (footing width B = 50 mm; thickness and slope height = 600 mm). The same inclination of model test slopes, 2(H):1(V), and geotextile sand were used in the prototype study. The software enabled the automatic generation of 6- or 15-node triangle plane strain elements for the soil.

**RESULTS AND DISCUSSION**

The load–settlement curves obtained from the experimental ultimate bearing capacity ( $q_u$ ) and the amount of settlement at the time of failure (S) were determined. Given the subsequent reduction of the bearing capacity of the slope, the bearing capacity reduction coefficient ( $j_\beta$ ) was determined as

$$j_\beta = \frac{q_u}{q_{u(\beta=0)}}$$

where  $q_{u(\beta=0)}$  was the ultimate bearing capacity of the strip footing on a flat surface (Figure 2). Table 1 shows the unreinforced test program. We investigated the following effects of geometrical parameters on the bearing capacity of strip footing on reinforced sand slope experiments (Figure 2):

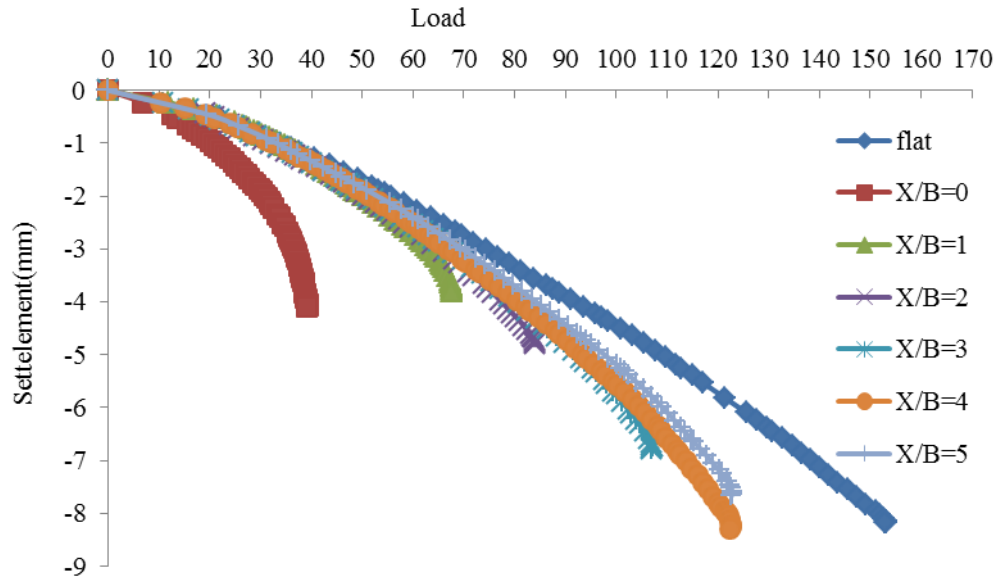
- (a) Ratio of depth of the first layer to the footing width (d/B).
- (b) Ratio of distance from the slope crest to the footing width (X/B).
- (c) Vertical spacing between layers to the footing width (h/B).

Table 1. The unreinforced test program.

Test No	$\beta^\circ$	Dr%	B (mm)	X/B
Ur1*	0	85	50	-
Ur2	30	85	50	0
Ur3	30	85	50	1
Ur4	30	85	50	2
Ur5	30	85	50	3
Ur6	30	85	50	4
Ur7	30	85	50	5
Ur8	30	85	70	0
Ur9	30	85	70	1
Ur10	30	85	70	2
Ur11	30	85	100	0
Ur12	30	85	100	1
Ur13	30	85	100	2
Ur14	30	85	150	0
Ur15	30	85	150	1
Ur16	30	85	150	2
Ur17	30	60	50	0
Ur18	30	60	50	1
Ur19	30	60	50	2
Ur20	30	60	70	0
Ur21	30	60	70	1
Ur22	30	60	70	2
Ur23	30	60	100	0
Ur24	30	60	100	1
Ur25	30	60	100	2
Ur26	30	60	150	0
Ur27	30	60	150	1
Ur28	30	60	150	2

- (d) Increase of width footing (B).
- (e) Number of reinforcement layers (N).

The behavior of bearing capacity and settlement of strip footing on reinforced slope was examined, as well as the bearing capacity values based on the sizes and types of equipment used for the tests. The multi-layer reinforced d



**Figure 3.** Load variations with settlement for different edge distances of strip footing on the slope ( $D_r=85\%$ , and  $\beta=30^\circ$ ).

was also obtained from the experiment. The optimum values of parameters  $h$  and  $N$  were used, which reinforced the basic parameters related to width  $B$ . The value calculated by the ratio ( $d/B$ ,  $h/B$ ,  $H_r/B$ , and  $X/B$ ) was expressed. To make the optimum values of the strip footing width  $B$  dimensionless, the experimental results evaluated the reinforcement. The load settlement curves obtained from the experiment, the ultimate bearing capacity, and the settlement values were determined at the time of failure. Given the reinforcement to express a given increase in bearing capacity, the bearing capacity ratio (BCR) can be expressed as follows:

$$BCR = \frac{q_{ur}}{q_u}$$

$q_{ur}$  : Reinforcement ultimate bearing capacity

$q_u$  : Non-reinforcement ultimate bearing capacity

The reinforcement that results from the decrease in settlement values is referred to as the settlement reduction factor (SRF), which can be expressed as follows:

$$SRF = \frac{S_r}{S}$$

$S_r$  : Settlement value of reinforced sand slope

$S$  : Settlement value of unreinforced sand slope

### Effect of edge distance of strip footing on bearing capacity

To investigate the footing on the slope, the laboratory experiments were placed at a total of seven different distances. In the experiments, footing width  $B = 50$  mm,  $\beta = 30^\circ$ , and  $D_r = 85\%$  were selected as the degree of firmness. Load ( $q$ ) and settlement ( $S$ ) curves are illustrated in Figure 3. The maximum values clearly showed the curve collapse load, which was determined as  $q_u$ . In the tapered case, with the value obtained from the payload, the payload will slope the value obtained from the ratio of the case by a factor of  $i_\beta$ . The  $q_u$  values in different  $X/B$  and the rates are summarized in Table 2. The relationship between  $X/B$  and  $i_\beta$  is illustrated in Figure 4. With a different edge distance of the strip footing on the slope, the following results were obtained from the experiments on the effects of bearing capacity.

With consideration for the distance of strip footing in selecting between the  $0B$  and  $5B$  experiments, the  $X/B$  ratio increased, and the value of the underlying bearing capacity increased the lateral support that was lost as a result of reactivating the entry. As a point was placed sufficiently far from the top, we beveled the remaining portion of the main ground floor. The failure occurred in the right wedge, which was partly because of passive resistance that increased the payload. The largest increase in bearing capacity  $X/B = 0$  and  $X/B = 1$  was between (19%) and  $X/B = 2$  with the constant distance increased significantly (10%). In  $X/B = 3$ , the value of state approximately corresponds to 70%. The increase in bearing capacity  $X/B = 4$  and  $X/B = 5$  showed a 1% decrease, and  $X/B = 5$  to 80% of the value of reaching

**Table 2.** Ultimate bearing capacity test results ( $D_r = 85\%$  and  $\beta = 30^\circ$ ).

X/B	qu(kN/m <sup>2</sup> )	S(mm)	i <sub>β</sub>
0	39.27	-4.06	0.256315
1	67.64	-3.72	0.441486
2	83.98	-4.75	0.548137
3	107.16	-6.74	0.699432
4	122.58	-8.22	0.800078
5	122.87	-7.59	0.801971
Flat	153.21	-8.16	1

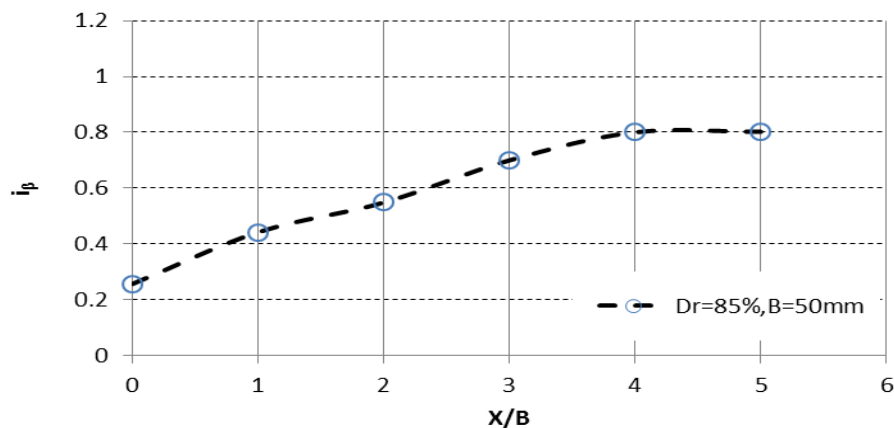


**Figure 4.** Bearing capacity of strip footing on different slope distances.

out. The effect of the payload was largely irrelevant. As the X/B value increased, the load settlement became steeper. With increasing curves and dips, the value of X/B is less than 4.

**Effects of number of geotextile layers on settlement**

The efficiency of reinforcement on the settlement of strip footing was investigated. Figure 5 illustrates the differences between the load–settlement curves of unreinforced and reinforced soil mass. The difference in ultimate bearing capacity was caused by the difference in the slope at the near end of the curves, which results in increased settlement by the increase of reinforced layers. The method of settlement calculated by the load settlement curve is presented in Figure 5. Table 3 provides the results obtained for ( $D_r = 85\%$ ,  $X/B = 1$ , and  $\beta = 30^\circ$ ).

As shown in Table 3, the foundation settlement increased with reinforcement. However, using one-layer reinforcement seems logical when increasing bearing capacity and allowable quantities of settlement are considered. Relative to other situations, reinforcement is unnecessary because both settlement of footing and the

bearing capacity increase. For example, the bearing capacity of soil mass with three-layer reinforcements and unreinforced soil was obtained (358.9/67.4). However, the settlement increased in the three-layer reinforcement, which was caused by the tension rupture of the soil confined between geotextile layers.

Comparisons of Table 3 and Figure 5 indicated similar results for the two cases of edge distance. Therefore, using reinforcement in sand slope with a large edge distance is beneficial because it increases bearing capacity, although the settlement increased compared with unreinforced soil. The settlement process is still increased by adding reinforcement layers. In investigating the effect of reinforcing the bearing of the number of layers, experimental studies showed that as the number of reinforcement layers (N) increased, so did the reinforced soil bearing capacity. The optimum reinforcement layer was found to be  $N = 3$ . In this case, the effective reinforcement depth ( $H_r$ ) is  $2.5 B$ . Figures 6 and 7 show that according to the optimum reinforcement layer, an increase of 3.2 times was observed in the number of loads.

An increasing number of reinforcement layers contribute significantly to the bearing capacity of the slope. The bearing capacity increased with the passive

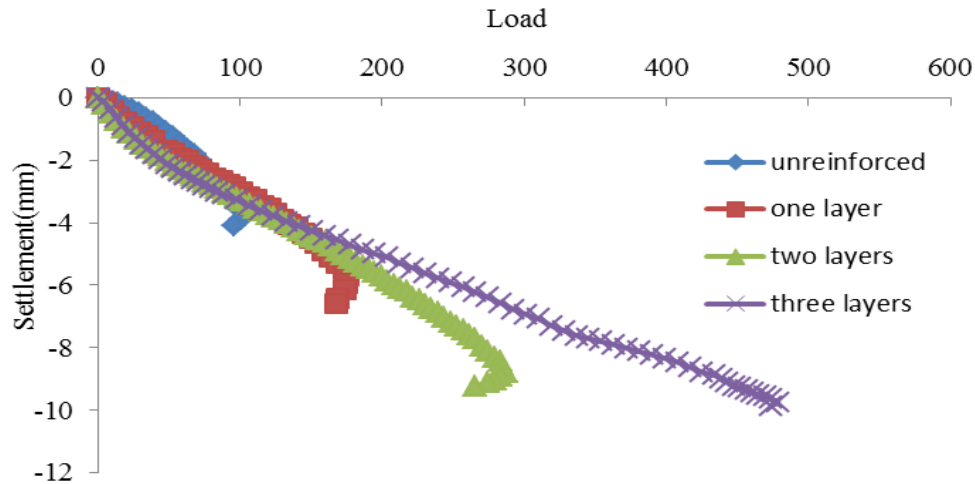


**Figure 5.** Load–settlement curves for different numbers of reinforcement layers at  $D_r = 85\%$ ,  $X/B = 2$ , and  $\beta = 30^\circ$ .

**Table 3.** Variation of footing settlement and bearing capacity for reinforcement soil.

Soil type	Bearing capacity	Footing settlement (mm)
Unreinforced	67.4	4.375
One reinforced layer	158.9	4.66
Two reinforced layers	283.5	6.7
Three reinforced layers	358.9	9.22

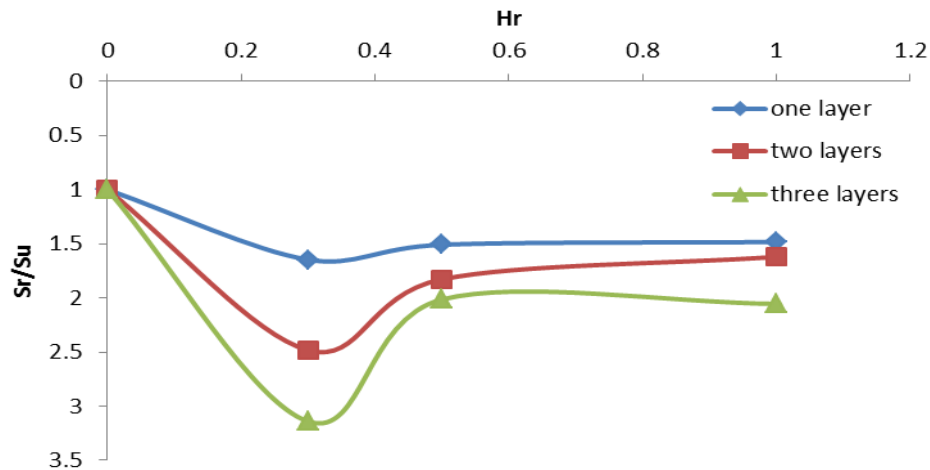


**Figure 6.** Variation of  $H_r$  with  $S_r/S_u$ .

resistance of the ground, which consists of sand, and the soil–geotextile reinforcement mechanism can be said to be due to adhesion. Reinforcement is composed of tensile, shear stresses below the footing against the horizontal layer, which exhibits resistance, and the stress shows a more stable soil layer that transfers a failure in a

wider and deeper zone.

Table 3 shows the value of  $q_u$  experiments, which corresponds to approximately the same value of  $q$  in sitting rates in unreinforced and reinforced cases. Figure 8 shows the  $H_r$ –SRF given relationship. Based on Table 3 and Figure 8, if strip footing is placed in the soil

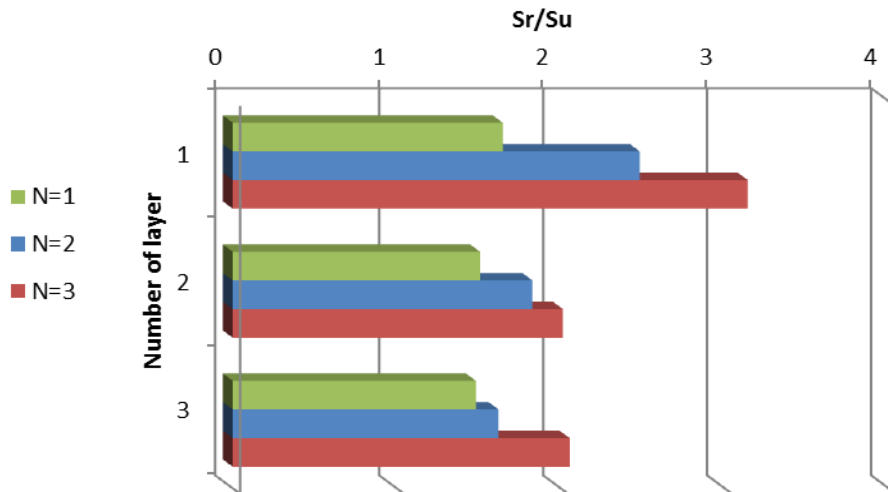


Figure 7. Variation of Sr/Su with number of layers.

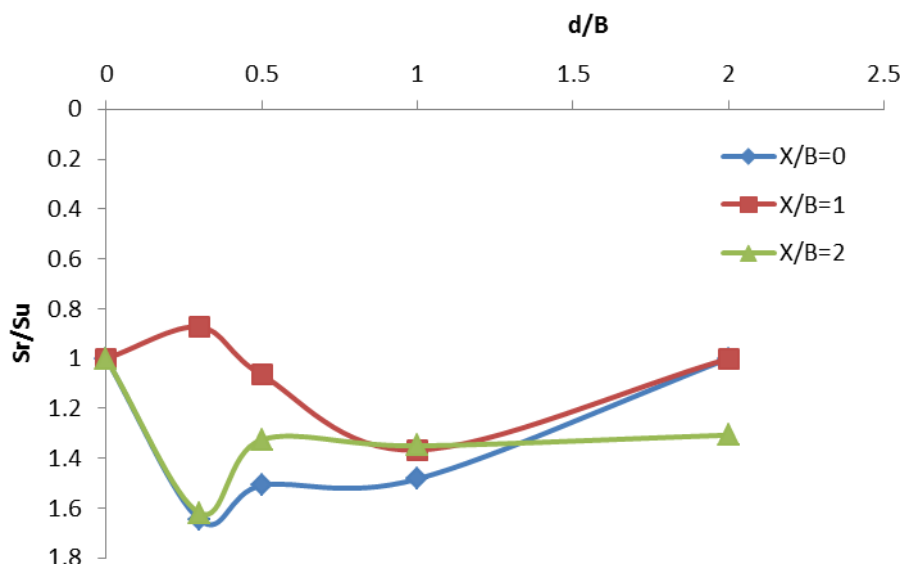


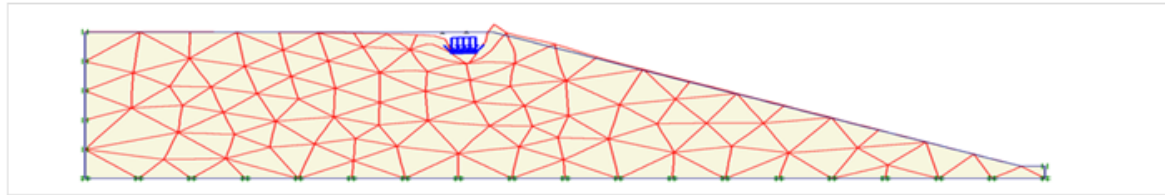
Figure 8. Variation of Sr/Su with depth of first layer.

reinforcement layer of  $N = 3$ , then the strip footing decreases under the same load values. The improvement in the strip behavior of the  $N = 3$  reinforcement reached approximately 45% of the value of the number of layers  $N = 4$ .

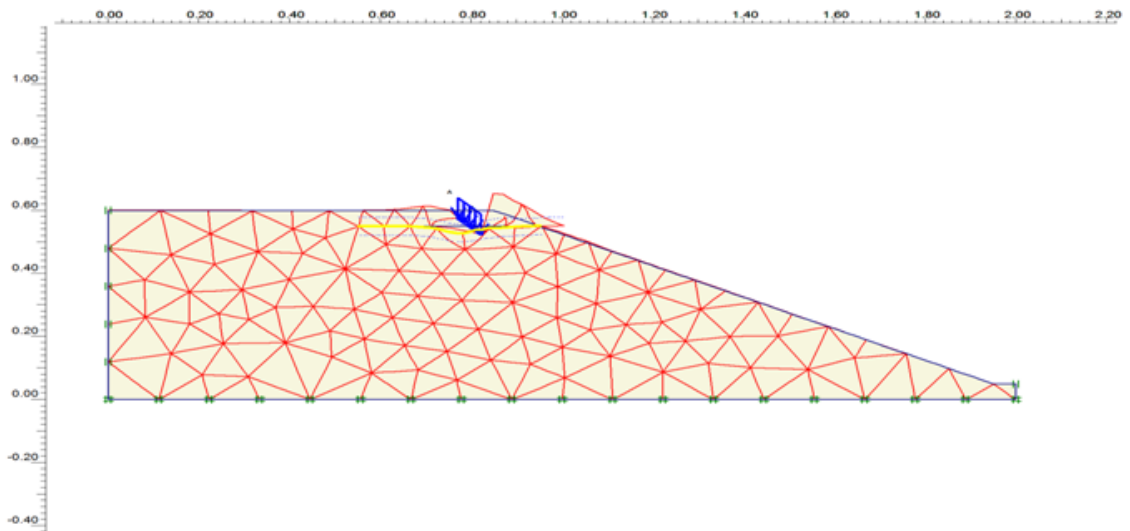
**FEA results**

FEA results are shown in Figures 9a to h. Figure 9a presents a typical deformed FE mesh for strip footing on reinforced sand slope in the case of ( $X/B = 1$ ,  $\beta = 30^\circ$ , and  $d/B = 0.5$ ). A small deformation is shown, which is a significant feature of the reinforced sand slope, unlike the

unreinforced case. The presence of geotextile significantly decreased the deformation of both underlying soil and slope compared with the footing without geotextile. This observation can be confirmed by the displacement vector obtained from the analysis and shown in the following figures 9b. The geotextile layers decreased subgrade deformation and prevented particles from moving to the region surrounded by the geotextile layer. The geotextile layers provide lateral restraint, which controls the horizontal movement of soil particles under the footing and mitigates slope deformation (Figure 9c). The geotextile layers also decrease the horizontal movement of subgrade particles. The extreme horizontal displacement also developed beyond the confined region

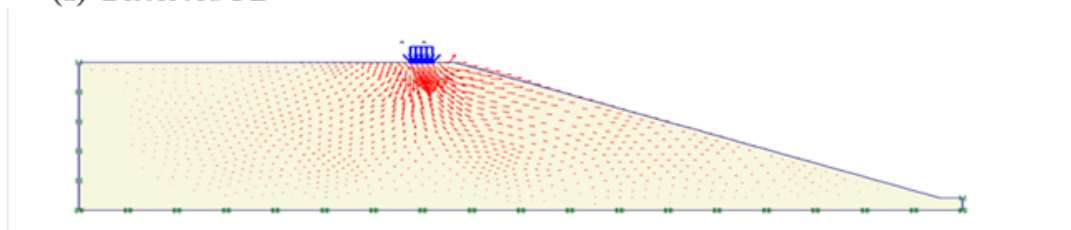


1) Without reinforcement

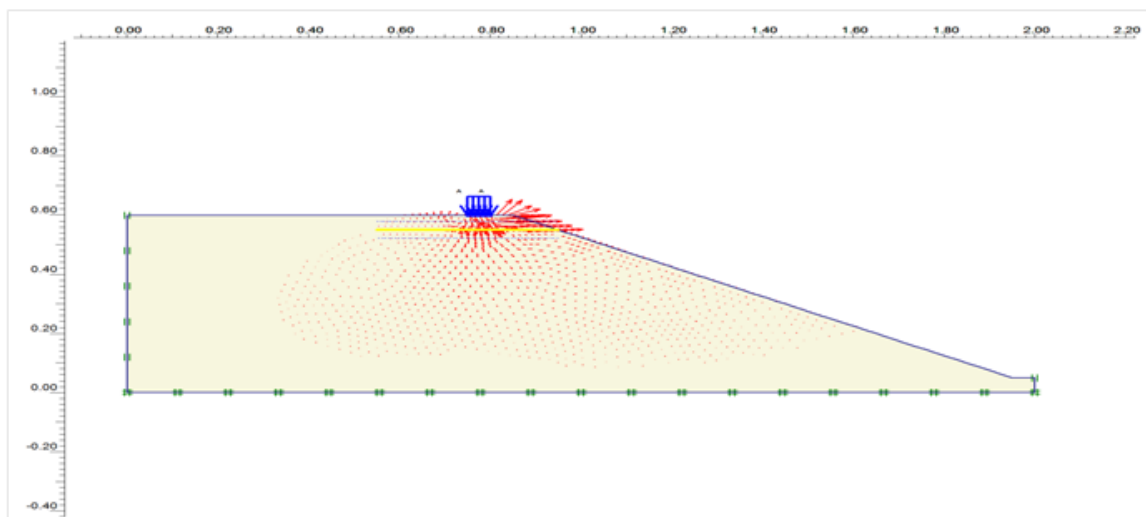


2) One-layer reinforcement

(a) Distorted FE

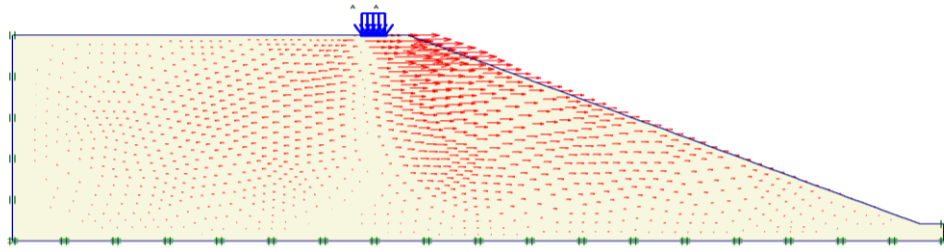


1) Without reinforcement

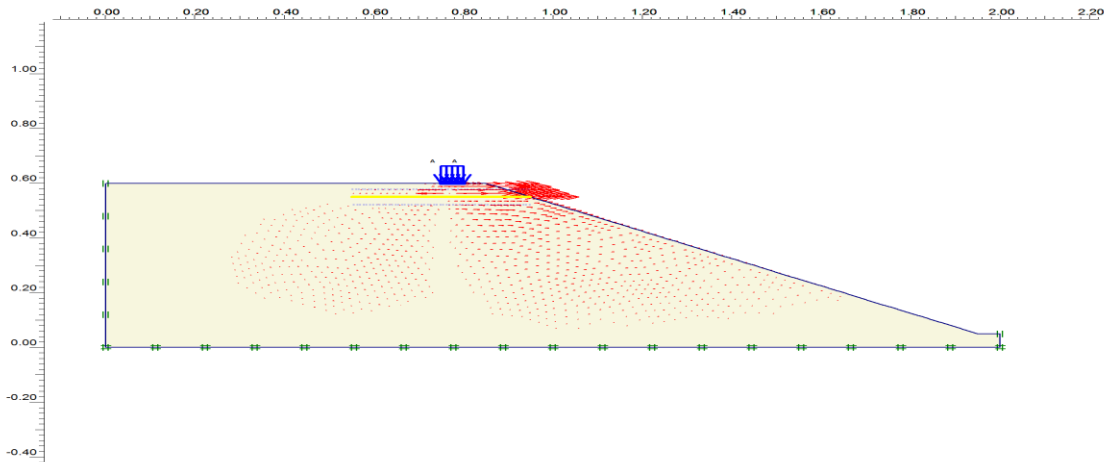


1) One-layer reinforcement

b) Total displacement vector

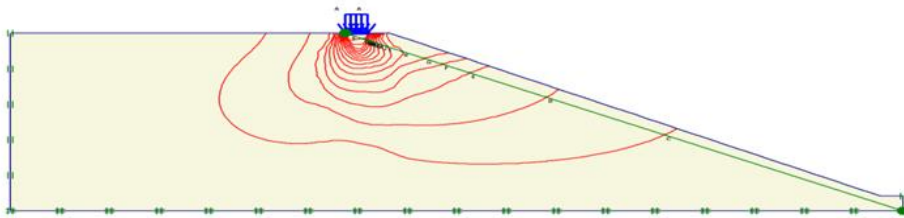


1) Without reinforcement

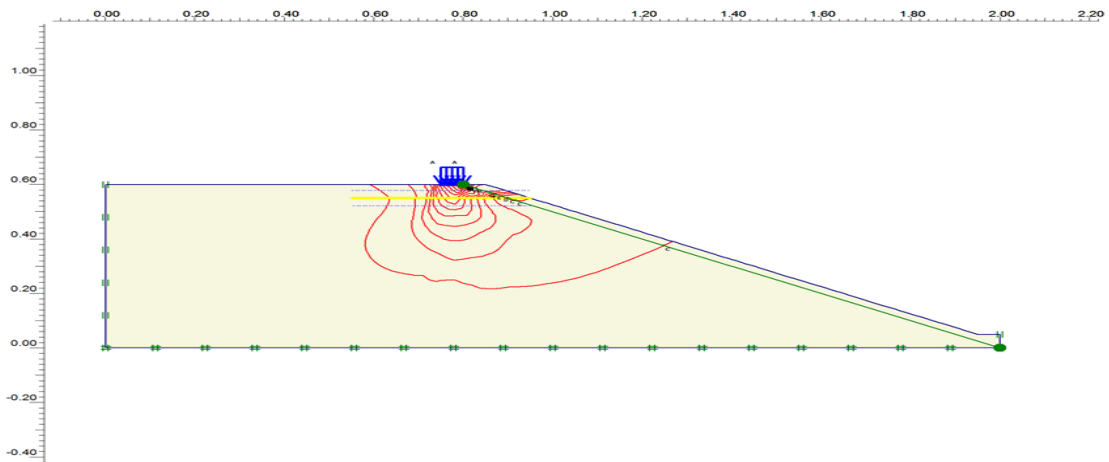


2) One reinforced layer

(c) The horizontal displacement vector

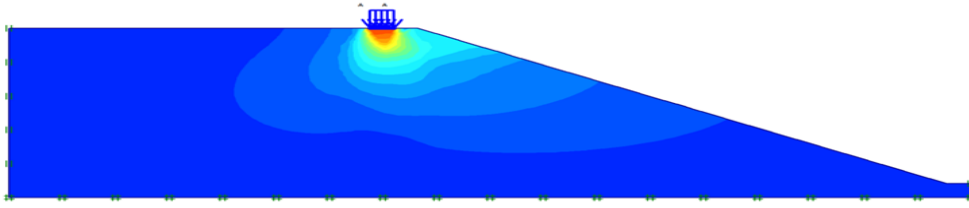


1) Without reinforcement

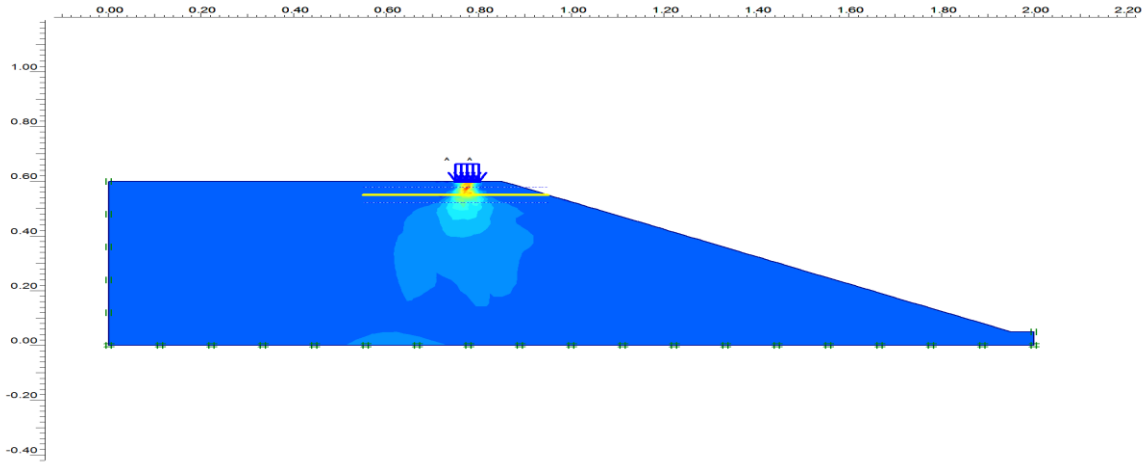


2) One reinforced layer

d) Horizontal displacement contours

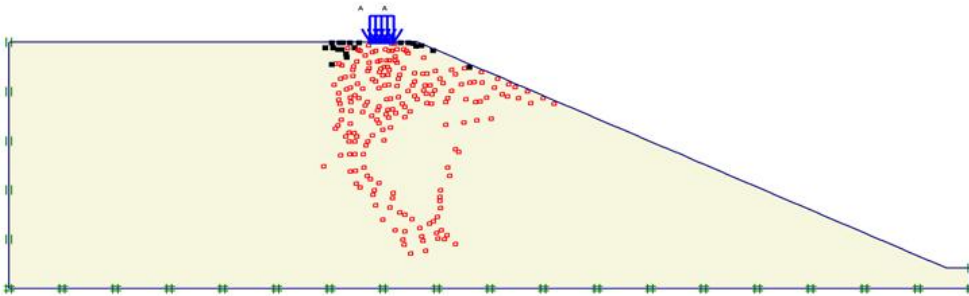


1) Without reinforcement

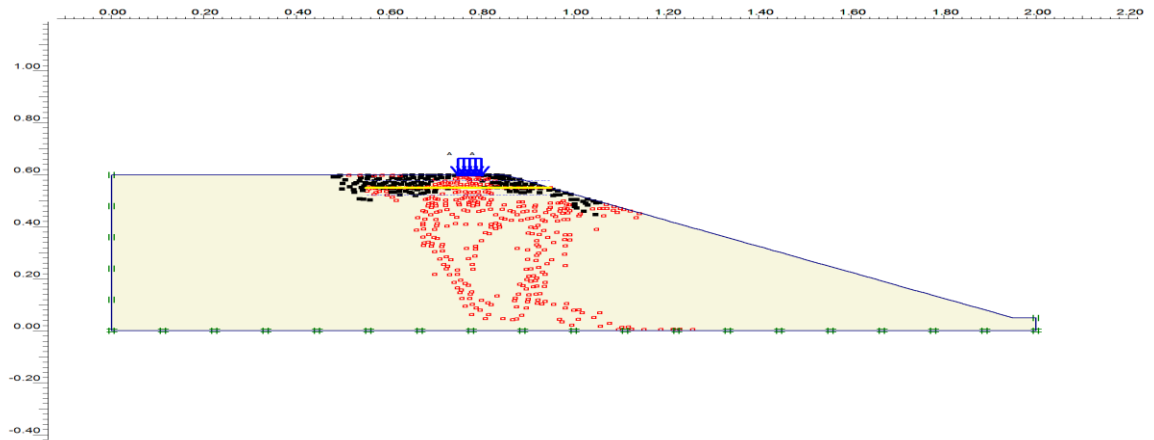


2) One-layer reinforcement

e) Shading of mean stresses

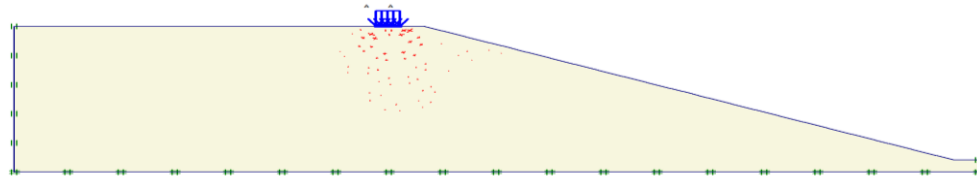


1) Without reinforcement

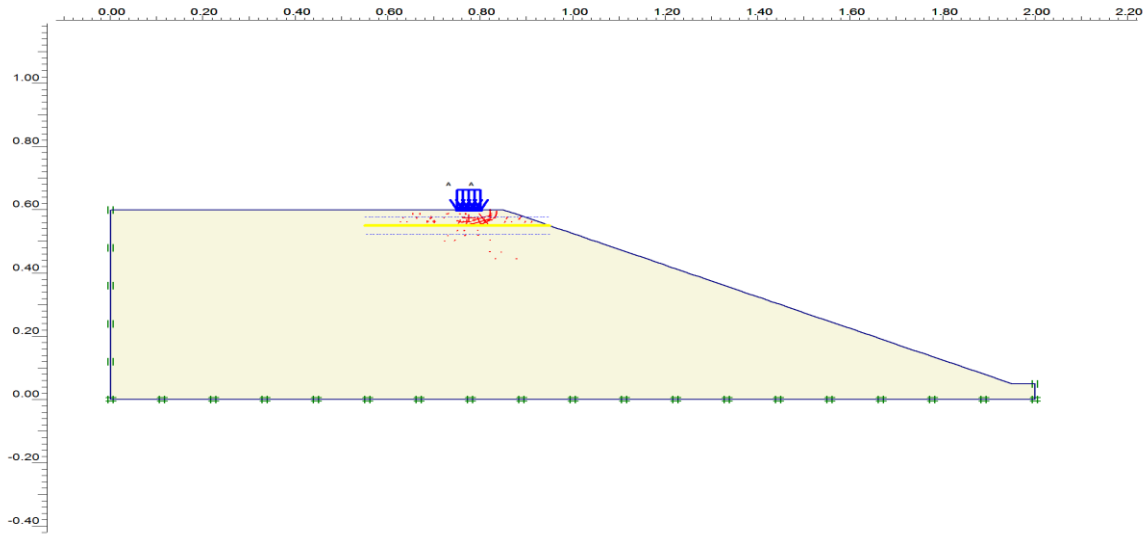


2) One-layer reinforcement

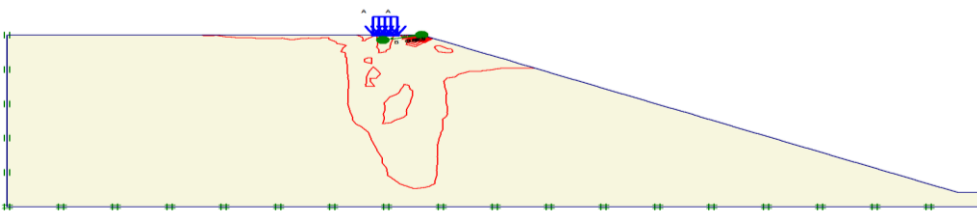
f) Plastic points for geotextile



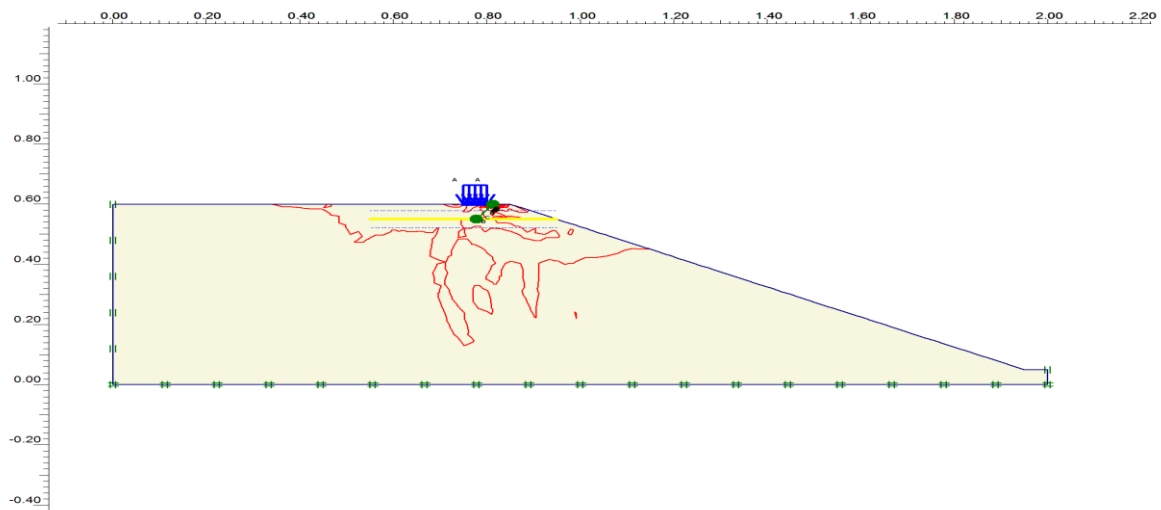
1) Without reinforcement



2) One-layer reinforcement  
(g) The principal strain location



1) Without reinforcement



2) One-layer reinforcement  
(h) The contours of principal strain

**Figure 9.** Horizontal displacement contours in soil mass under footing placed on: (a) unreinforced slope, (b) reinforced footing ( $d=B$ ).

(Figure 2d), which exhibits contours of extreme horizontal displacement. Figure 2d identifies slope zones in which subgrade particles have a large horizontal displacement. The displacement was mainly observed at the zones located below the confined subgrade and was extended vertically within a distance of nearly  $0.5 B$  (Figure 9d). The convergence between the contours was densely located below the confined zone.

Generally, horizontal displacement of the confined particles is almost null when geotextile layers are located beyond depth  $2 B$ . As the depth of the reinforcement layer decreases, the horizontal movement of the subgrade increases to the outside region. Thus, slope deformation also increases. The geotextile layers provide lateral restraint, which modifies the stress distribution zone under the base (Figure 9e). The extreme values were located between the following.

The stress shading denotes the absence of resistance in the soil adjacent to the slope as a result of the slope effect (left side). However, resistance on the right part was observed because the shading in the adjacent soil increased densely as the geotextile layer transmitted the stress to the soil. This observation can be confirmed by plastic or stress point distribution along both sides of the geotextile layer, which was observed along the length of the geotextile layer.

Figure 9f shows the distribution of the plastic points beneath the footing with the geotextile layer. Plastic points are referred to as stress points in the plastic states, which can be observed mainly at the zone above the geotextile layer. Small plastic points are illustrated below the region, which indicates that shear failure can be expected at the outside region below the reinforcement layer. This observation also indicated that soil shear failure occurred mostly beyond the reinforcement layer as expected. Moreover, the shear strains decreased through the reinforced zone (Figure 9g), which represents the distribution of the principle shear strains. As also shown in Figure 9g, the geotextile layer transferred the stress to the adjacent soil, which produced strains at each edge. This finding indicates that geotextile layers have a considerable effect on decreasing shear stress in the reinforced zone. In addition, the contours of shear strains (Figure 9h) indicate that shear failure will develop at the end of the reinforced region.

Given that the main contours were extended below the reinforced soil, shear failure developed in a deeper location. The location where the maximum shear strain converged was regarded as a slip surface where shear failure initiates. Propagation of the high-strain zone at the end of the reinforced region caused progressive failures.

Figure 9 shows that the load transfer mechanism occurs in a deeper zone below the geotextile layer, which explains the occurrence of shear failure. The main function of the reinforcement layer is to reduce the distortion rate in the sheared zone and the ultimate shear

stress mobilized in the shear zone. Thus, the bearing capacity failure can be modified to punch the shear failure under the footing, and the general bearing capacity failure occurred at the top geotextile layer.

### Comparison between experimental and numerical results

Initially, the numerical model used the results obtained from the experimental test program of this study. Figure 10 shows a comparison between the BCR values obtained from FEA and the results obtained from the experimental model tests. FEA results have a reasonable fit with the experimental data and are in accordance with the same trend. Figure 10 also shows the experimental and numerical results of three tests:  $X/B = 0$ ,  $X/B = 1$ , and  $X/B = 2$ . Although the numerical results do not fit completely with the experimental results, the results are in good agreement. Any discrepancy may be related to the chosen model, soil, and foundation parameters, and differences between the boundary conditions in the numerical and experimental models.

Figure 11 shows the typical results of load curves for the strip footing tests on sand slope. The results were obtained from the bearing capacity tests on sand slope at a density of  $D_r = 85\%$ . The failure modes for each of the footings varied depending on the sand type and density. The curves showed that large strip footings have a higher bearing capacity than small strip footings, which was also the case for tests on each density. The results also indicated that values of  $N_y$  for sand decreased with the footing size and increased higher relative density. The relative density also had a significant influence on  $N_y$  (Figure 12). The results shown in Figure 12 suggest that as the footing width decreased,  $N_y$  increased significantly faster than that which was previously noted.

The failure mode of the footings varied depending on density and footing size. To explain the observed different behaviors, the footings were related to the critical state concept. The concept suggests that dense sand under large mean stresses tend to contract. The same concept can be related to footings of different widths. For example, if four footings of various sizes were placed on the same sand in the same state and in the influence area, the mean stress of the four footings would be different. The largest footing would have the largest influence area, and the smallest footing would have the smallest influence area.

The bearing capacity factor  $N_y$  depends on the absolute width of the footing for strip footing (Figure 12). The  $N_y$  for strip footing decreased with the footing size but increased with the increasing relative density. One explanation for the scale effect is stress dependency, in which different footing sizes have different mean stresses, which means that a smaller footing indicates a smaller mean stress. The observation is related to the

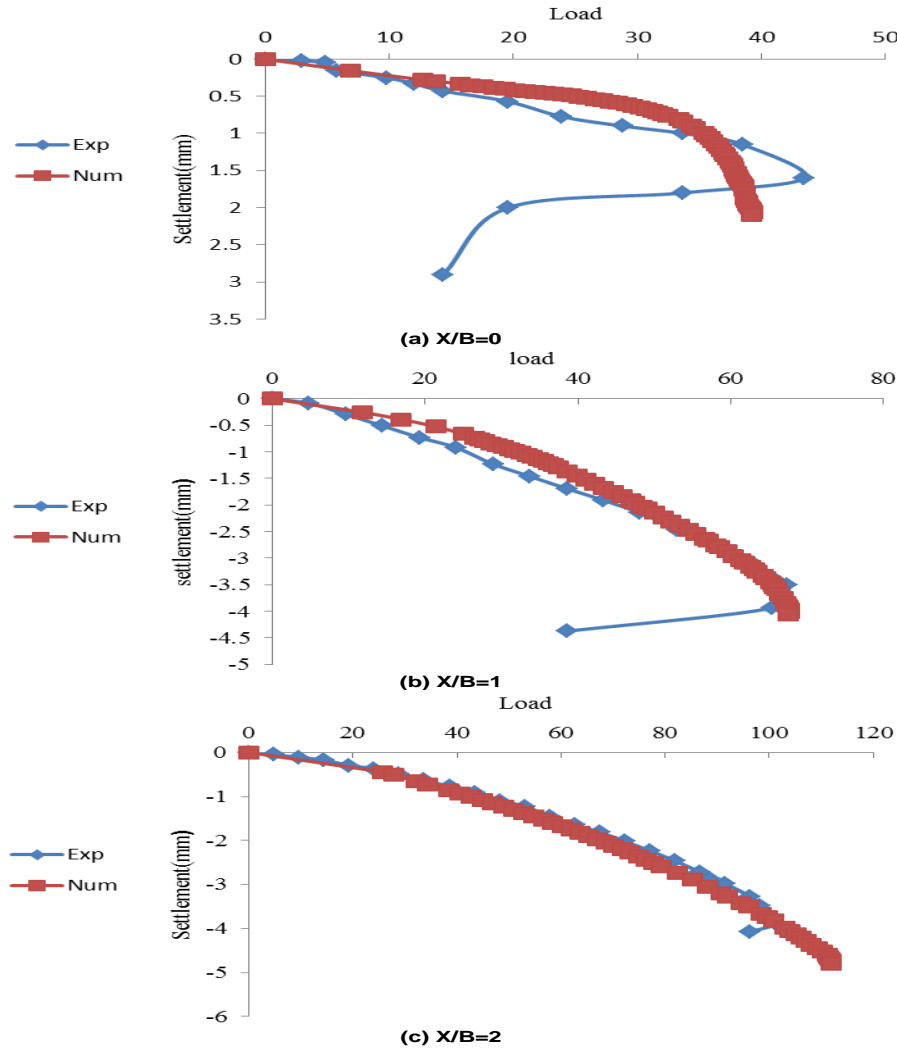


**Figure 10.** Experimental and numerical results of test with  $D_r=85\%$  (a)  $X/B = 0$ ; (b)  $X/B = 1$ ; and (c)  $X/B = 2$ .

critical state strength. A small footing (small mean stress) would function as if it was on denser soil than a larger footing, despite being tested on sand with the same void ratio. The stress dependency may also be related to the curvature of the Mohr–Coulomb failure envelope where high friction angles at low stresses and low friction angles at high mean stresses were observed. The curvature of the Mohr–Coulomb failure envelope has been widely documented and can explain why small footings have large  $N_\gamma$  values. Thus, large friction angles correspond to the dense state of soil in relation ( $\Psi$ ) to the critical state line.

**Effect of  $\Psi$  on bearing capacity factor  $N_\gamma$**

The bearing capacity factor  $N_\gamma$  depends on the soil unit weight  $\gamma$  and can be calculated by assuming

cohesionless soil ( $C = 0$ ) with no surcharge ( $q = 0$ ). The generalized Terzaghi’s bearing capacity equation is given as:

$$q_u = \frac{1}{2} B \gamma N_\gamma$$

where  $N_\gamma$  is the bearing capacity factor for strip footing.

Table 4 lists the values of the bearing capacity factor  $N_\gamma$  for  $X/B = 0.0, 1.0,$  and  $2.0$ , which shows the variation of  $N_\gamma$  with  $\Psi, X/B,$  and  $B$  for strip footing. Figure 13 shows the variation of  $N_\gamma$  with  $B$  and  $\Psi$  for strip footing widths of 50, 70, 100, and 150.  $N_\gamma$  increased considerably with increasing  $X$ . The dilatancy had a significant effect on the value of the bearing capacity factor, particularly for high  $X$

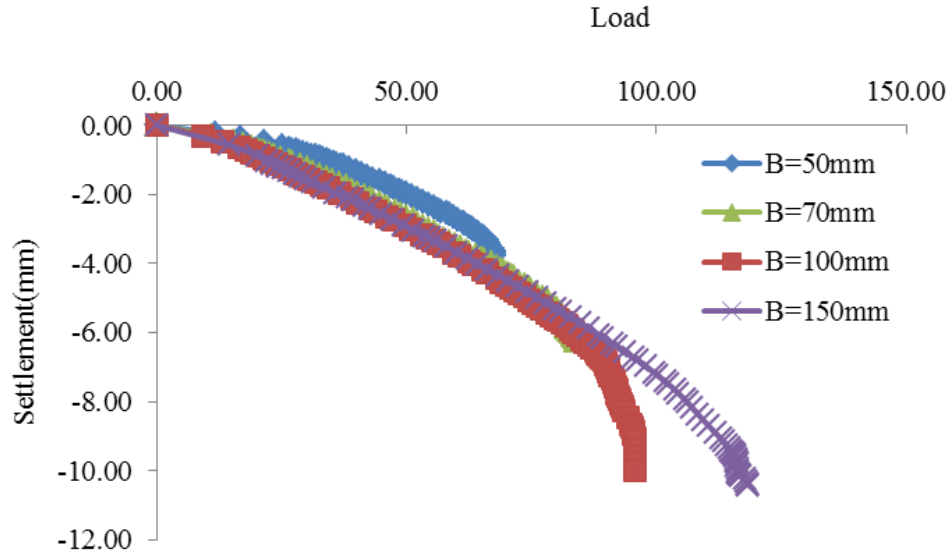


Figure 11. Load variations with S for model slope with different footing widths ( $X/B=1$ ).

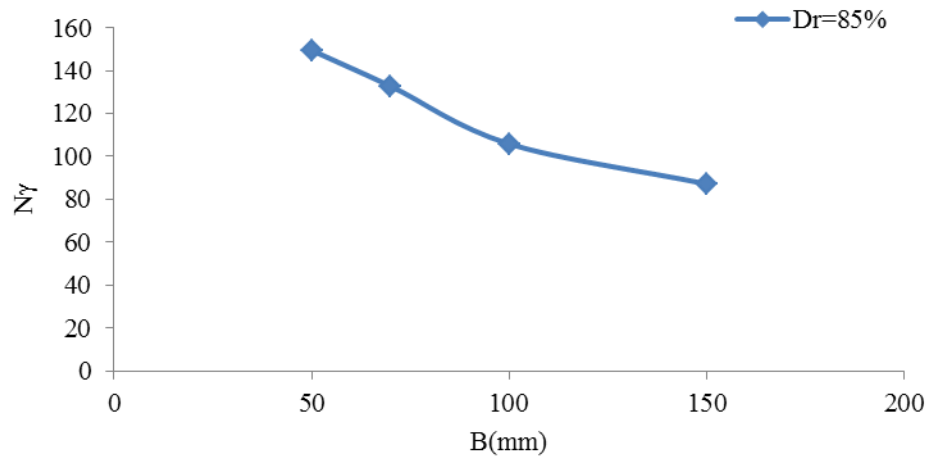


Figure 12.  $N_y$  versus B for 85% relative density.

Table 4. Bearing capacity factor  $N_y$  for strip footing on sand slope with relative density of 60%.

X/B	B(mm)	$N_y$				
		$\psi$				
		0	$\phi/4$	$\phi/2$	$3\phi/4$	$\phi$
(0)	50	58.93491	69.5858	76.21302	77.15976	82.36686
	70	37.19358	51.05664	62.21471	62.72189	63.90533
	100	24.26036	37.75148	41.30178	45.08876	46.0355
	150	5.443787	28.00789	31.3215	34.00394	34.47732
(1)	50	69.5858	91.59763	104.142	108.6391	109.3491
	70	25.86644	79.79713	88.25021	90.78614	92.98394
	100	21.06509	59.40828	63.07692	70.88757	72.42604
	150	33.13609	44.26036	49.78304	52.70217	53.57002

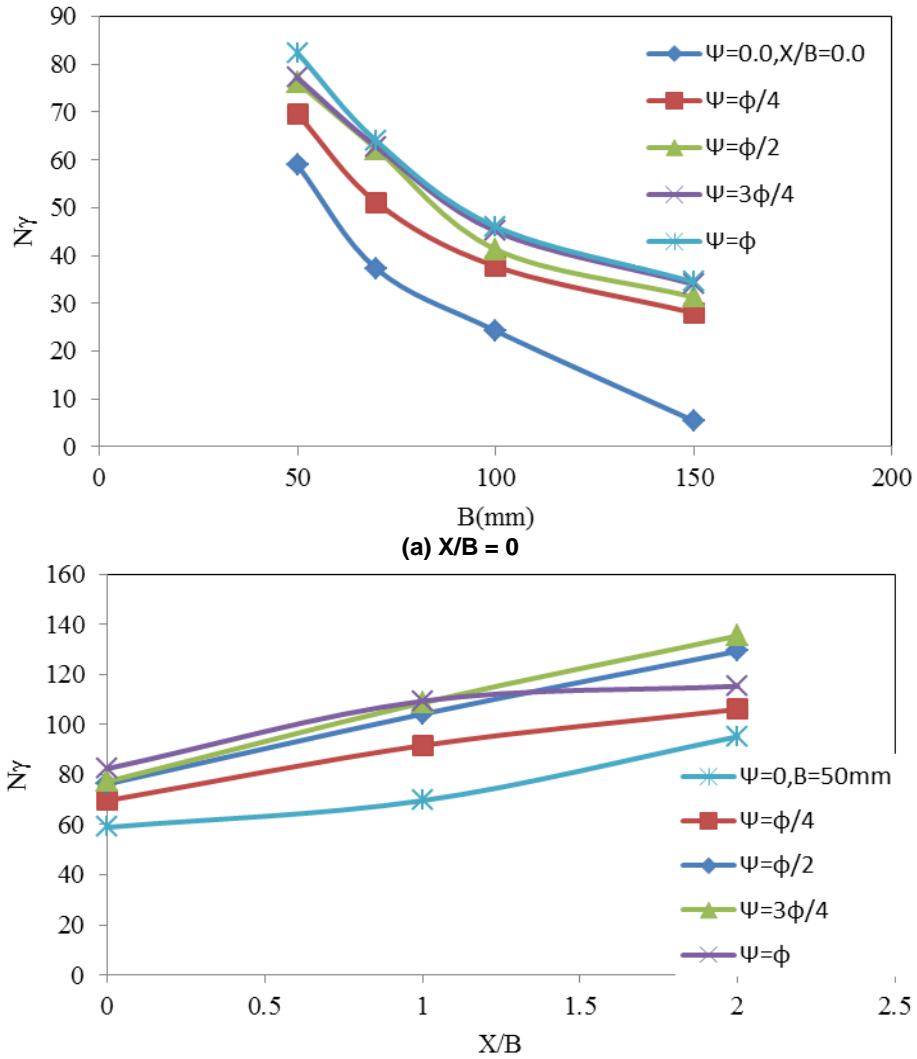


Figure 13.  $N_y$  versus  $X/B$  for different  $\phi$  for relative density of 60%.

values.  $N_y$  decreased significantly when  $\Psi$  decreased.

The gap between the two values of  $N_y$  increased with the increase of  $X$ . The decrease of  $N_y$  was evident when the value of  $\Psi/\phi$  decreased from  $3/4$  to  $0$ . Beyond this limit, the decrease seemed to be insignificant.

**Conclusions**

A series of experimental and numerical model tests was conducted to evaluate the bearing capacity of a strip footing with and without reinforcement that rests adjacent to the crest of sand slopes. This study mainly aimed to investigate the effects of geotextile depth, footing location, and slope angle on both ultimate bearing

capacity and failure mechanism. Based on our findings, the following conclusions can be drawn:

1. Stabilizing the earth slope by using geotextile at an adequate depth in conjunction of the strip footing adjacent to the slope crest had a significant effect on improving soil bearing capacity.
2. The optimum geotextile depth that produced the maximum ultimate bearing capacity was approximately 0.5 of the footing width.
3. The ultimate bearing capacity of a strip footing with geotextile increased with increasing distance from the footing to the edge and decreased when the angle of slope increased. However, at an edge distance greater than the footing width, the ultimate bearing capacity effectively increased.
4. FEA helped to better explain the failure patterns of the footing-reinforced soil system adjacent to a slope. FEA

also confirmed the load transfer mechanism and illustrated how geotextile can protect the slope from collapsing by decreasing the slope deformation.

## REFERENCES

- Adams MT, Collin JG (1997). Large Model Spread Footing Load Tests on Geosynthetic Reinforced Soil Foundation. *J. Geotech. Geoenviron. Eng.* 123(1):66-72.
- Akinmusuru JO, Akinbolade JA (1981). Stability of Loaded Footings on Reinforced Soil. *J. Geotech. Eng.* 107:819-827.
- Banimahd M, Woodward PK (2006). Load-displacement and bearing capacity of foundations on granular soils using a multi-surface kinematic constitutive soil model. *Int. J. Numer. Anal. Methods Geomech.* Wiley 30:865-886.
- Bathurst RJ, Blatz JA, Burger MH (2003). Performance of Instrumented Large-Scale Unreinforced and Reinforced Embankments Loaded by a Strip Footing to Failure. *Canadian Geotech. J.* 40:1067-1083.
- Berry DS (1935). Stability of Granular Mixtures. American Society for Testing Materials: Proceedings of the 38th Annual Meeting. 35(2):491-507.
- Binquet J, Lee KL (1975a). Bearing Capacity Tests on Reinforced Earth Slabs. *J. Geotech. Eng. Div. ASCE.* 101(12):1241-1255.
- Bolton MD, Lau CK (1989). Scale Effects in the Bearing Capacity of Granular Soils. Proceedings of the 12th International Conference on Soil Mechanics and Foundation Engineering. 2:895-898.
- Cerato AB, Lutenegeger AJ (2007). Scale effects of shallow foundation bearing capacity on granular material. *J. Geotech. Geoenviron. Eng.* 133(10):1192-1202.
- Chang CS, Cerato AB, Lutenegeger AJ (2010). Modelling the scale effect of granular media for strength and bearing Capacity. *Int. J. Pavement Eng.* 11(5):343-353.
- Clark JI (1998). The settlement and bearing capacity of very large foundations on strong soils: the 1996 R. M. Hardy lectures. *Canadian Geotech. J. Ottawa* 35:131-145.
- Das BM, Omar MT (1994). The effects of foundation width on model tests for the bearing capacity of sand with geogrid reinforcement. *Geotech. Geol. Eng.* 12:133-141
- De Beer EE (1963). The scale effect in the transposition of the results of deep-sounding tests on the ultimate bearing capacity of piles and caisson foundations. *Geotechnique*, 13(1):39-75.
- Dixit RK, Mandal JN (1993). Bearing Capacity of Geosynthetic-Reinforced Soil Using Variational Method. *Geotextiles and Geomembranes*, 12(6):543-566.
- El Sawwaf M, Nazir AK (2010). Behavior of repeatedly loaded rectangular footings resting on reinforced sand. *Alexandria Eng. J.* 49(4):349-356.
- El Sawwaf M, Nazir AK (2012). Cyclic settlement behavior of strip footings resting on reinforced layered sand slope. *J. Adv. Res.* 3(4):315-324.
- El Sawwaf ME (2007). Behavior of Strip Footing on Geogrid-Reinforced Sand over a Soft Clay Slope. *Geotextiles and Geomembranes*, 25(1):50-60.
- Fragaszy RJ, Lawton EC (1984). Bearing Capacity of Reinforced Sand Subgrades. *J. Geotech. Eng.* 110:1500-1507.
- Guido VA, Chang DK, Sweeny MA (1985). Comprasion of Geogrid and Geotextile Reinforced Slabs. *Canadian Geotech. J.* 23:435-440.
- Huang C, Tatsuoka F, Sato Y (1994). Failure mechanisms of reinforced sand slopes loaded with a footing. *Soils and Foundations* 24(2):27-40.
- Huang CC, Tatsuoka F (1990). Bearing Capacity of Reinforced Horizontal Sandy Ground. *Geotextile Geomembranes*, 9:51-82.
- Khing KH, Das BM, Puri VK, Cook EE, Yen SC (1993). Bearing Capacity of a Strip Foundation on Geogrid-Reinforced Sand. *Geotextile and Geomembranes*, 12(4):351-361.
- Kumar A, Saran S (2003). Closely Spaced Footings on Geogrid-Reinforced Sand. *J. Geotech. Geoenviron. Eng. ASCE* 129(7):660-664.
- Kumar A, Walia BS (2006). Bearing Capacity of Square Footings on Reinforced Layered Soil. *J. Geotech. Geological Eng.* 24:1001-1008.
- Kumar J, Bhoi MK (2008). Interference of Multiple Strip Footings on Sand Using Small Scale Model Tests. *Geotech. Geol. Eng.* 26:469-477.
- Kusakabe O (1995). Chapter 6: Foundations. *Geotechnical Centrifuge Technology*, R. N. Taylor, ed., Blackie Academic & Professional, London, 118-167.
- Kusakabe O, Yamaguchi H, Morikage A (1991). Experiment and Analysis on the Scale Effect of Ny for Circular and Rectangular Footings. *Centrifuge 1991*. pp. 179-186.
- Laman M, Yildiz A (2003). Model Studies of Ring Foundations on Geogrid-Reinforced Sand. *Geosynthetics International*, Thomas Telford, 10(5):142-152.
- Laman M, Yildiz L, Keskin MS, Uncuoğlu E (2007). Donatılı Kum Seve Oturan Serit Temelin Deneysel Olarak İncelenmesi. *ĐMO Teknik Dergi*, 277:4197-4217.
- Lancelot L, Shahrouf I, Mahmoud MA (2006) Failure and dilatancy properties of sand at relatively low stresses. *J. Eng. Mech. ASCE* 132(12):1396-1399
- Lee KM, Manjunath VR (2000). Experimental and Numerical Studies of Geosynthetic-Reinforced Sand Slopes Loaded with a Footing. *Canadian Geotech. J.* 37:828-842.
- Mandal JN, Sah HS (1992). Bearing Capacity Tests on Geogrid-Reinforced Clay. *Geotextile and Geomembranes*, 11(3):327-333.
- Michalowski RL (2004). Limit Loads on Reinforced Foundation Soils. *J. Geotech. Geoenviron. Eng.* 130(4):381-390.
- Moghaddas SN, Dawson AR (2010). Behavior of footings on reinforced sand subjected to repeated loading – comparing use of 3D and planar geotextile. *Geotextiles and Geomembranes* 28:434-447.
- Moghaddas TSN, Khalaj O (2008). Laboratory tests of small-diameter HDPE Pipes buried in reinforced sand under repeated load. *Geotextiles and Geomembranes*. 26(2):145-163.
- Plaxis (2002). User Manual. 2D version8, (Edited by BRINKGREEVE, R.J.B.), Delft University of Technology & PLAXIS b.v., The Netherlands.
- Selvedurai APS, Gnanendran CT (1989). An Experimental Study of a Footing Located on a Sloped Fill: Influence of a Soil Reinforcement Layer. *Canadian Geotech. J.* 26(3):467-473.
- Shiraishi S (1990). Variation in bearing capacity factors of dense sand assessed by model loading tests. *Soil and Foundations*, 30(1):17-26.
- Tatsuoka F, Okahara M, Tanaka T, Tani K, Morimoto T, Siddiquee MSA (1991). Progressive failure and particle size effect in bearing capacity of footing on sand. *Geotechnical Engineering Congress 1991*. McLean, F., Campbell, D.A., and Harris, D.W., Editors, ASCE Geotechnical Special publication No.27, Vol.2, Proc. Congress held Boulder, Colorado, USA, June 1991, pp. 788-802.
- Tatsuoka F, Siddiquee MSA, Tanaka T (1994). Link among design, model tests. Theories and sand properties in the bearing capacity of footing on sand. 13th Int. Conf. Soil Mechanics Foundations Eng. New Delhi, India, 1:87-88.
- Vidal H (1968). La Terre Arme. *Annales de L'Institut Technique du Batiment et des Travaux Publics*: 888-938 (as referred by Das, 1999).
- Yetimoğlu T, Wu JTH, Saglamer A (1994). Bearing Capacity of Rectangular Footings on Geogrid-Reinforced Sand. *J. Geotech. Eng.* 120(12):2083-2099.
- Yoo C (2001). Laboratory Investigation of Bearing Capacity Behavior of Strip Footing on Geogrid-Reinforced Sand Slope. *Geotextiles and Geomembranes*, 19:279-298.
- Zhu F, Clark JI, Phillips R (2001). Scale effect of strip and circular footings resting on dense sand. *J. Geotechnol. Geoenviron. Eng. ASCE* 127(7):613-621.